Available online at www.sciencedirect.com

SciVerse ScienceDirect

Journal of the European Ceramic Society 32 (2012) 2459–2467

www.elsevier.com/locate/jeurceramsoc

Preparation of (0 2 0)-oriented $BaTi_2O_5$ thick films and their dielectric responses

Akihiko Ito *, Dongyun Guo, Rong Tu, Takashi Goto

Institute for Materials Research, Tohoku University, 2-1-1 Katahira, Aoba-ku, Sendai 980-8577, Japan

Received 4 January 2012; received in revised form 15 February 2012; accepted 16 February 2012
Available online 13 March 2012

Abstract

Barium dititanate ($BaTi_2O_5$) thick films were prepared on a Pt-coated Si substrate by laser chemical vapor deposition, and ac electric responses of (0 2 0)-oriented $BaTi_2O_5$ films were investigated using several equivalent electric circuit models. $BaTi_2O_5$ films in a single phase were obtained at a Ti/Ba molar ratio ($m_{Ti/Ba}$) of 1.72–1.74 and deposition temperature (T_{dep}) of 908–1065 K as well as $m_{Ti/Ba} = 1.95$ and $T_{dep} = 914$–953 K. (0 2 0)-oriented $BaTi_2O_5$ films were obtained at $m_{Ti/Ba} = 1.72$–1.74 and $T_{dep} = 989$–1051 K. $BaTi_2O_5$ films had columnar grains, and the deposition rate reached 93 $\mu m\,h^{-1}$. The maximum relative permittivity of the (0 2 0)-oriented $BaTi_2O_5$ film prepared at $T_{dep} = 989$ K was 653 at 759 K. The model of an equivalent circuit involving a parallel combination of a resistor, a capacitor, and a constant phase element well fitted the frequency dependence of the interrelated ac electrical responses of the impedance, electric modulus, and admittance of (0 2 0)-oriented $BaTi_2O_5$ films.

Keywords: Films; $BaTiO_3$ and titanates; Impedance; Dielectric properties; $BaTi_2O_5$

1. Introduction

Ferroelectricity of barium dititanate ($BaTi_2O_5$, BT_2) has not been realized until recently despite considerable study on the BaO–TiO_2 quasi-binary system. We first prepared a ferroelectric $BaTi_2O_5$ single crystal and reported its high relative permittivity along the *b*-axis ($\varepsilon' = 20{,}000$) and its high Curie temperature ($T_C = 750$ K).[1,2] The first-principle calculation showed that the piezoelectric response of $BaTi_2O_5$ is comparable to that of $PbTiO_3$; thus, $BaTi_2O_5$ is a promising candidate for a new lead-free ferroelectric material.[3] Since piezoelectric force is directly related to film thickness, a *b*-axis-oriented $BaTi_2O_5$ thick film is required to achieve a large mechanical force in a practical actuator.

Although the preparation of $BaTiO_3$ films by chemical vapor deposition (CVD) has been extensively studied because of its wide use in ferroelectric devices such as capacitors and actuators,[4–8] the preparation of $BaTi_2O_5$ films by CVD has rarely been reported. Yu et al. reported the formation of the $BaTi_2O_5$ phase in their study of $BaTiO_3$ epitaxial growth by aerosol CVD[9]; however, the ferroelectricity of $BaTi_2O_5$ was not yet realized. To study $BaTi_2O_5$ films, we prepared ferroelectric $BaTi_2O_5$ epitaxial thin films by laser ablation[10]; however, its deposition rate around 0.1 $\mu m\,h^{-1}$ should be increased to prepare thick $BaTi_2O_5$ films for practical applications. Laser chemical vapor deposition (laser CVD) is advantageous to obtain oriented and thick $BaTi_2O_5$ films at a high deposition rate. Laser CVD preparation of Y_2O_3–ZrO_2, Al_2O_3 and CeO_2 thick films was demonstrated at high deposition rates of more than several hundreds of micrometer per hour with significant orientation growth.[11–13]

For the characterization of dielectric materials, ac impedance spectroscopy has been widely used. Although the ac electric response has been conventionally analyzed by a Debye-type relaxation process using the equivalent electric circuit model involving a parallel combination of resistor (R) and capacitor (C) elements, deviations from the Debye-type response are commonly observed. Thus, a non-Debye-type element,[14] the so-called constant phase element (CPE), has often been used to explain these deviations. Masó et al. recently proposed an equivalent circuit model involving a parallel combination of R, C and the CPE to characterize the frequency-dependent electrical responses of the $BaTi_2O_5$ single crystal,[15] in which the CPE would correlate with cooperative dipolar interactions.

* Corresponding author. Tel.: +81 22 215 2106; fax: +81 22 215 2107.
E-mail address: itonium@imr.tohoku.ac.jp (A. Ito).

0955-2219/$ – see front matter © 2012 Elsevier Ltd. All rights reserved.
doi:10.1016/j.jeurceramsoc.2012.02.022

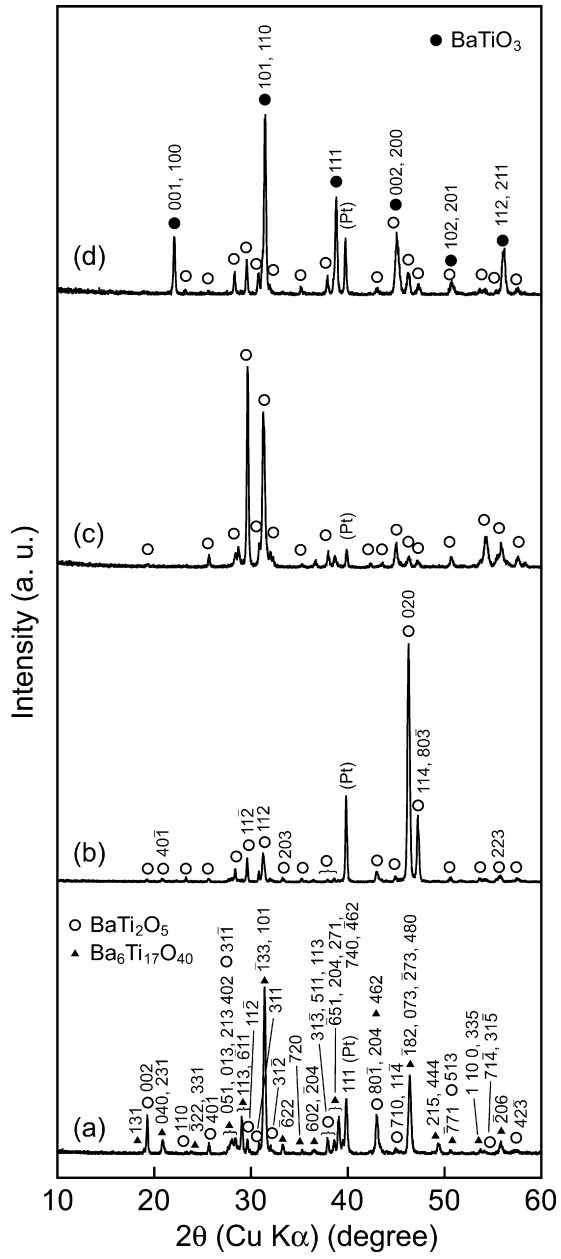

Fig. 1. XRD patterns of Ba–Ti–O films prepared at various $m_{Ti/Ba}$ and T_{dep}: 1.95 and 1020 K (a), 1.74 and 978 K (b), 1.74 and 957 K (c), and 1.06 and 1014 K (d), respectively.

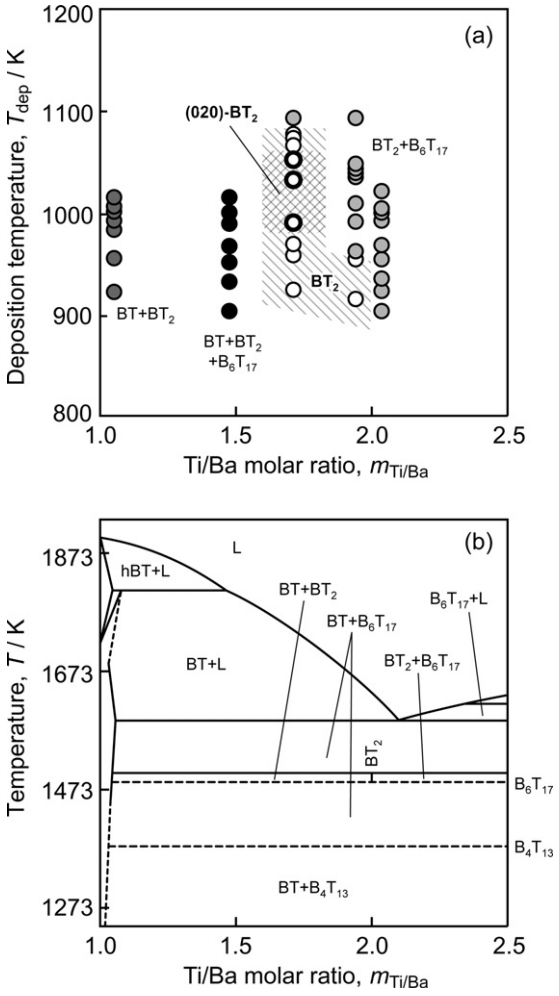

Fig. 2. Effects of Ti/Ba molar ratio and deposition temperature on the phase of Ba–Ti–O films (a), The hatched area indicates optimal deposition conditions for single-phase $BaTi_2O_5$ films. Phase diagram for the BaO–TiO_2 quasi-binary system (b).[16]

In the present study, we have prepared (0 2 0)-oriented $BaTi_2O_5$ thick films on a Pt-coated Si substrate by laser CVD, and the ac electric responses of the films were investigated using several equivalent electric circuit models.

2. Experimental procedure

$BaTi_2O_5$ thick films were prepared on a Pt-coated Si substrate by laser CVD with a continuous-wave mode Nd:YAG laser (wavelength: 1064 nm). Details of the laser CVD apparatus and the procedure have been reported elsewhere.[12] The substrate was placed on a hot stage, and a thermocouple was inserted near the substrate to measure the deposition temperature (T_{dep}). The substrate was heated on a hot stage at a pre-heating temperature (T_{pre}) of 773 K. A laser beam 15 mm in diameter was introduced through a quartz window to irradiate the entire substrate. As the laser power (P_L) increased from 52 to 93 W, T_{dep} increased from 918 to 1092 K. Barium dipivaloylmethanate ($Ba(dpm)_2$) and titanium diisopropoxy-dipivaloylmethanate ($Ti(OiPr)_2(dpm)_2$) precursors were evaporated at 563 K and 433–444 K, respectively. Their vapors were carried into a chamber with Ar gas, and O_2 gas was separately introduced into the chamber through a double-tube gas nozzle. The total pressure (P_{tot}) in the chamber was maintained at 400 Pa. Deposition was conducted for 600 s.

The crystal phase of the films was analyzed by X-ray diffraction (XRD, Rigaku RAD-2C) using Cu Kα X-ray radiation. The surface and cross-sectional microstructure of these films was observed by a scanning electron microscope (SEM, Hitachi S-3100H), and their dielectric properties were measured by an ac impedance spectroscope (Hewlett-Packard HP4194) in air from 298 to 1100 K in a frequency range between 2×10^2 and 10^6 Hz. Gold paste was used as an electrode. The ac electric responses

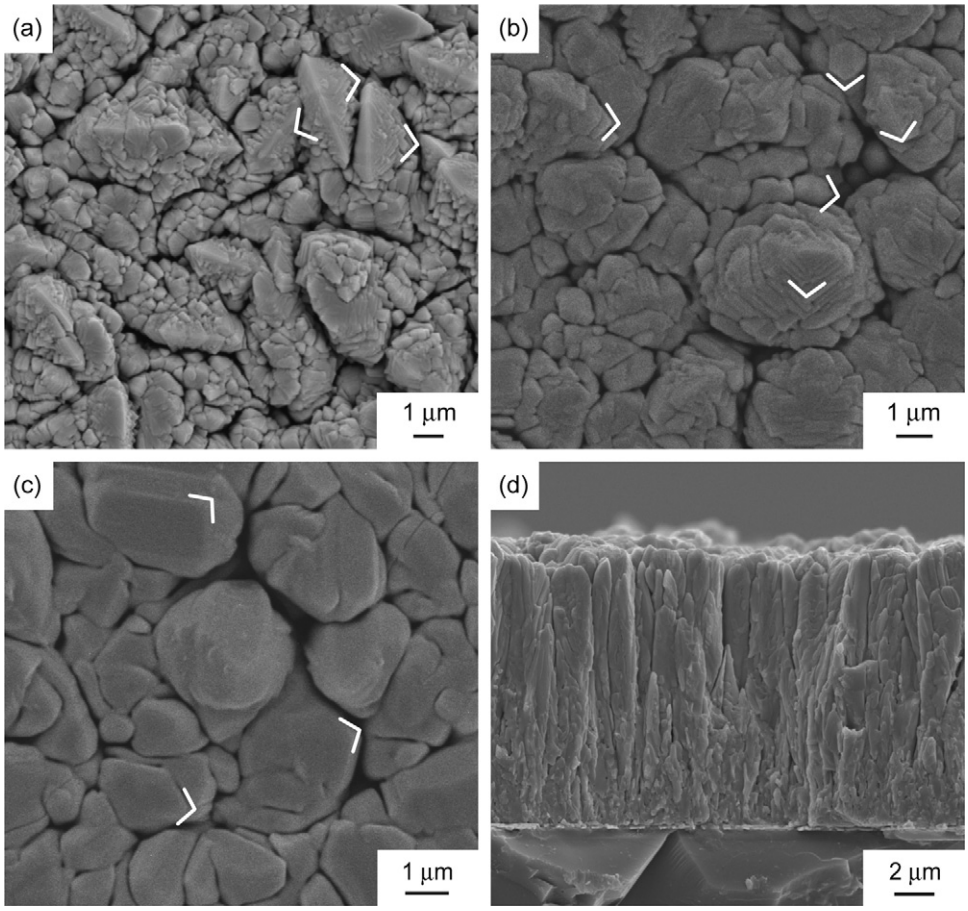

Fig. 3. Surface morphologies of $BaTi_2O_5$ films prepared at T_{dep} = 973 K (a), 989 K (b), and 1028 K (c); cross-sectional microstructure of the film prepared at 989 K (d).

from the equivalent circuit models were calculated using ZView (Scribner Associates), an equivalent circuit modeling software.

3. Results and discussion

3.1. Preparation of (0 2 0)-oriented $BaTi_2O_5$ films

The Ti/Ba molar ratio ($m_{Ti/Ba}$) in source vapor was calculated from the weight change of each precursor. Increasing the evaporation temperature of the Ti precursor from 438 to 444 K resulted in an increase in $m_{Ti/Ba}$ from 1.06 to 2.04.

Fig. 1 shows the XRD patterns of Ba–Ti–O films prepared at various $m_{Ti/Ba}$ and T_{dep}. A mixture phase of $BaTi_2O_5$ and $Ba_6Ti_{17}O_{40}$ was formed at $m_{Ti/Ba}$ = 2.04 and T_{dep} = 890–1001 K as well as $m_{Ti/Ba}$ = 1.95 and T_{dep} = 961–1092 K (Fig. 1(a)). $BaTi_2O_5$ films in a single phase were obtained at $m_{Ti/Ba}$ = 1.95 and T_{dep} = 914–953 K as well as $m_{Ti/Ba}$ = 1.72 − 1.74 and T_{dep} = 908–1065 K. $BaTi_2O_5$ films prepared at T_{dep} = 989–1051 K showed significant (0 2 0) orientation (Fig. 1(b)), whereas the $BaTi_2O_5$ films prepared below 989 K showed (1 1 $\bar{2}$) and (1 1 2) co-orientation (Fig. 1(c)). At T_{dep} = 1092 K, the $Ba_6Ti_{17}O_{40}$ phase was formed with the $BaTi_2O_5$ phase. At $m_{Ti/Ba}$ = 1.48 and T_{dep} = 902–1014 K, the films were a mixture phase of $BaTiO_3$, $BaTi_2O_5$, and $Ba_6Ti_{17}O_{40}$. In addition, a mixture phase of $BaTiO_3$ and $BaTi_2O_5$ was obtained at $m_{Ti/Ba}$ = 1.06 and T_{dep} = 921–1014 K (Fig. 1(d)). The (0 2 0) orientation degree of $BaTi_2O_5$ films prepared at $m_{Ti/Ba}$ = 1.72–1.74 and T_{dep} = 918–1092 K was evaluated using the Lotgering factor ($f_{(020)}$) as calculated from Eqs. (1) and (2):

$$f_{(020)} = \frac{P_m - P_0}{1 - P_0}, \tag{1}$$

$$P = \frac{I_{(020)}}{\sum I_{(hkl)}} \tag{2}$$

where P_m and P_0 are the XRD intensity ratios of the (0 2 0) $BaTi_2O_5$ plane to the summation of all (h k l) planes for measured and non-oriented specimens, respectively. P_0 was calculated from JCPDS card #72-3822.[17] The Lotgering factor has a value between 0 (non-oriented) and 1 (completely oriented). $BaTi_2O_5$ films showed (0 2 0) orientation ($f_{(020)}$ = 0.30–0.33) at T_{dep} = 989–1051 K.

Fig. 2(a) depicts the effects of $m_{Ti/Ba}$ and T_{dep} on the phase of Ba–Ti–O films. Single-phase $BaTi_2O_5$ films were obtained at $m_{Ti/Ba}$ = 1.72–1.74 and T_{dep} = 908–1065 K as well as $m_{Ti/Ba}$ = 1.95 and T_{dep} = 914–953 K. (0 2 0)-oriented $BaTi_2O_5$ films were obtained at $m_{Ti/Ba}$ = 1.72–1.74 and T_{dep} = 989–1051 K. $Ba_6Ti_{17}O_{40}$ was formed with $BaTi_2O_5$ at $m_{Ti/Ba}$ = 1.49–1.94 and $BaTiO_3$ with $BaTi_2O_5$ at $m_{Ti/Ba}$ < 1.49.

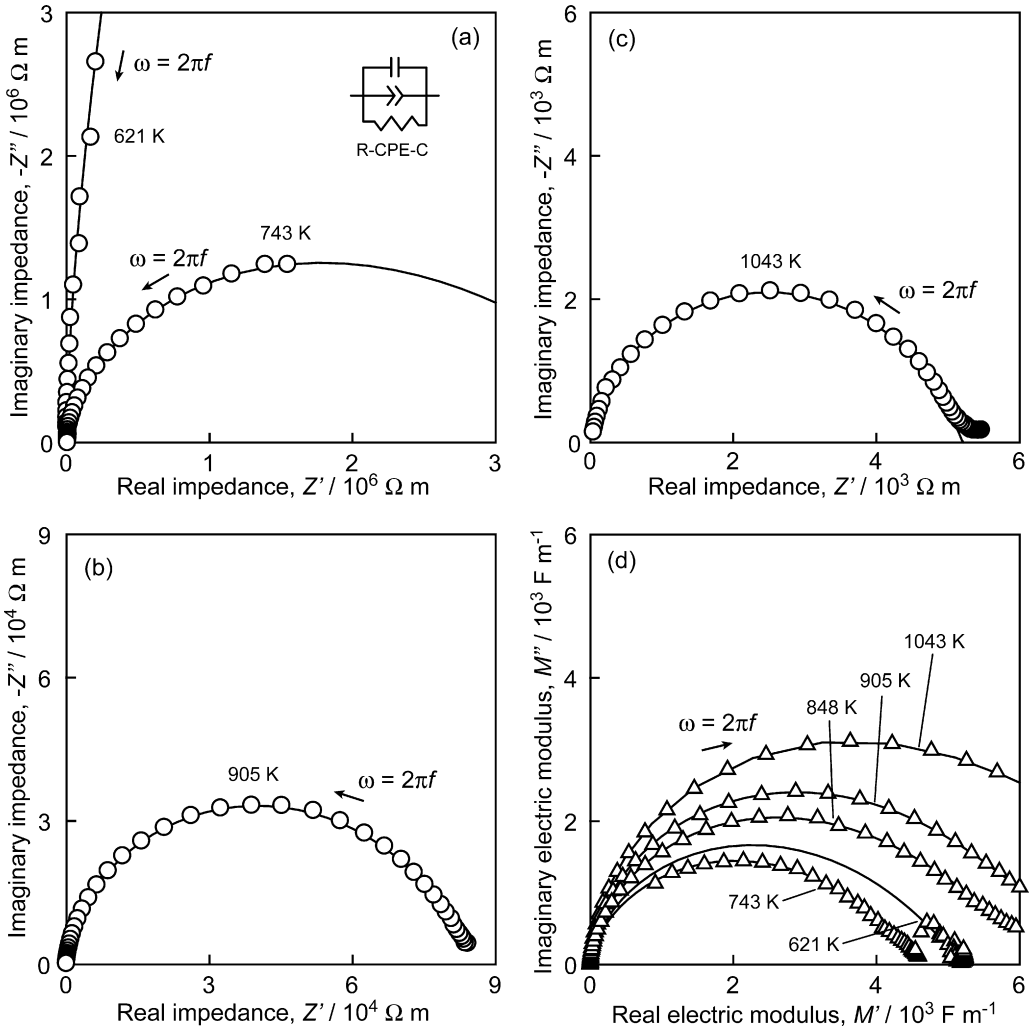

Fig. 4. Impedance complex plane plots for (0 2 0)-oriented $BaTi_2O_5$ films prepared at T_{dep} = 989 K measured at 621 and 743 K (a), 905 K (b), and 1043 K (c), and their electric modulus complex plane plots for these films (d). Solid lines represent curve fittings from the equivalent R–CPE–C parallel circuit (inset in (a)).

Fig. 2(b) shows the phase diagram for the BaO–TiO_2 quasi-binary system.[16] Although $m_{Ti/Ba}$ of single-phase $BaTi_2O_5$ films was slightly lower than that shown in the phase diagram, the trend of phase formation corresponded to that shown in the phase diagram.

It is known that $BaTi_2O_5$ is unstable at a high temperature and decomposes to $BaTiO_3$ and $Ba_6Ti_{17}O_{40}$; however, the stable temperature range of the $BaTi_2O_5$ phase is not well known. Statton first found the formation of the needle-like $BaTi_2O_5$ single crystal in the solidified specimen made from $BaCO_3$, TiO_2, and $BaCl_2$ ternary liquid and reported that the crystal congruently melted at 1676 K.[16] Rase and Roy published a phase diagram for the BaO–TiO_2 quasi-binary system including a $BaTi_2O_5$ phase,[17] and reported that $BaTi_2O_5$ can be produced by a solid-state reaction and solidification from a liquid phase and it decomposed below 1483 K and above 1605 K. Thereafter, several phase diagrams of BaO–TiO_2 were reported by Negas et al.[18] and O'Bryan and Thomson.[19] Since they regarded $BaTi_2O_5$ as a metastable phase, the $BaTi_2O_5$ phase was not described in their phase diagrams. The $BaTi_2O_5$ phase was not shown in the phase diagrams[18–23] until the discovery of the ferroelectricity of $BaTi_2O_5$,[1,24] which has focused renewed attention on its crystal structure, formation kinetics, dielectric properties and thermal stability.[2,3,25] Zhu and West recently reported a phase diagram in which $BaTi_2O_5$ can be an equilibrium phase in a narrow temperature range between 1493 and 1507 K.[26] By using a sol–gel method and precipitation on a solution using alkoxide precursors, the $BaTi_2O_5$ phase was formed above 973 K.[22,27] The stability range of $BaTi_2O_5$ is still controversial. In the present study, the single-phase $BaTi_2O_5$ films were obtained at T_{dep} = 918–1092 K.

Fig. 3 shows surface and cross-sectional SEM images of the $BaTi_2O_5$ films prepared at $m_{Ti/Ba}$ = 1.72 and various T_{dep}. The $BaTi_2O_5$ films prepared at T_{dep} = 973 K had a clamshell-like microstructure (Fig. 3(a)), and plate-like facets appeared on the surface of the grains. On the surface of the (0 2 0)-oriented $BaTi_2O_5$ film prepared at T_{dep} = 989 K, the grains had a rhombic terrace (Fig. 3(b)). At T_{dep} = 1028 K, the grain shapes became truncated (Fig. 3(c)). The inner angle of the rhombic terrace was almost identical to angle β of monoclinic $BaTi_2O_5$ (space group: $C2$; a = 1.6899 nm, b = 0.3935 nm, c = 0.9410 nm, β = 103.0°; ICSD #28-1548), as shown by the white lines in Fig. 3(b).[25]

This morphology indicates that the (0 2 0) $BaTi_2O_5$ plane grew perpendicular to the surface. In addition, the plate-like facets on the clamshell-like grains (Fig. 3(a)) and the truncated grains (Fig. 3(c)) had inner angles corresponding to angle β. The cross-sectional microstructure of $BaTi_2O_5$ films was columnar (Fig. 3(d)). The deposition rates of $BaTi_2O_5$ films were approximately 90 μm h^{-1} and almost independent of T_{dep}. The highest deposition rate of (0 2 0)-oriented $BaTi_2O_5$ films reached 93.3 μm h^{-1}, which was more than 100 times higher than those reported for the (0 2 0)-oriented $BaTi_2O_5$ films prepared by laser ablation[10] and the $BaTiO_3$ films by CVD.[28,29]

3.2. Dielectric responses of (0 2 0)-oriented $BaTi_2O_5$ films

Fig. 4 shows the impedance (Z^*) and electric modulus (M^*) complex plane plots measured at several temperatures for the (0 2 0)-oriented $BaTi_2O_5$ film prepared at T_{dep} = 989 K. At temperatures below 743 K, only a part of the impedance semicircle was observed due to the high electrical resistivity of the $BaTi_2O_5$ film (Fig. 4(a)). Electrical resistivity decreased with increasing temperature, and thus all semicircular responses were observed in the Z^* complex plane plot at measurement temperatures of 905 and 1043 K (Fig. 4(b) and (c), respectively). Similarly, in the M^* complex plane plot, the arc-shaped response became semicircular with increasing temperature (Fig. 4(d)). Since the electric modulus is the reciprocal of the relative permittivity ($\varepsilon^* = (M^*)^{-1}$), it showed minima around Curie temperature (T_C) 750 K.

An equivalent circuit model involving parallel combination of R and C elements is generally used to explain the ac response of dielectric materials, which results in semicircular curves in the Z^* and M^* complex plane plots. However, the impedance response plotted in the Z^* complex plane are often depressed from the ideal Debye-type response. The CPE can be used to express a non-Debye-type response.[14] The impedance response of the CPE is defined by Eq. (3):

$$Z^* = Q(j\omega)^{-n}, \tag{3}$$

where Q denotes the CPE constant, j is the imaginary unit, ω is the angular frequency and n is the CPE power parameter ($0 \le n \le 1$). The CPE becomes a pure capacitor when $n = 1$ ($Q = C$), whereas it becomes resistive (less capacitive) with decreasing n. For example, a parallel R–CPE circuit reproduces a depressed semicircular response in the Z^* complex plane plot, whose center is inclined at an angle of $(1 - n)\pi/2$.[14] The equivalent circuit of the $BaTi_2O_5$ single crystal has been studied by a parallel combination of R, C and CPE.[15] Solid lines in Fig. 4 show the calculated response of the equivalent R–CPE–C parallel circuit with fitted parameters. The R–CPE–C model well fitted the experimental data shown in the Z^* and M^* complex plane plots.

Fig. 5 shows the M'' and Z'' spectroscopic plots of the (0 2 0)-oriented $BaTi_2O_5$ film prepared at T_{dep} = 989 K and at several temperatures. A single peak was observed in both the M'' and Z'' plots, and the peak frequency increased with increasing temperature. The peak frequency of Z'' was slightly lower than that of M'' (arrows in Fig. 5(b)). The peak frequencies of Z'' and M'' should be the same in the case of a single RC parallel circuit element because

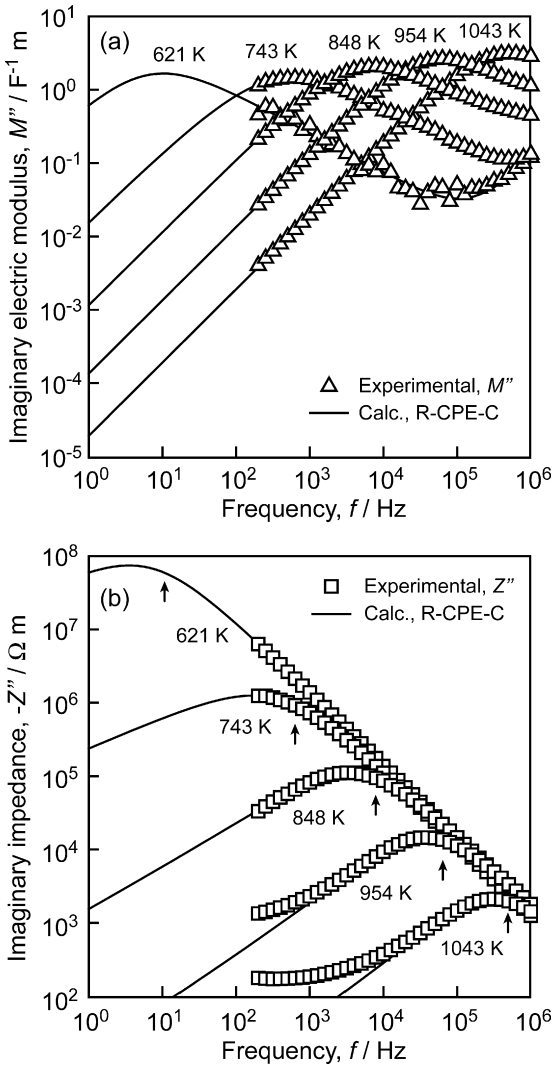

Fig. 5. Imaginary electric modulus (a) and imaginary impedance (b) as functions of frequency for the (0 2 0)-oriented $BaTi_2O_5$ film prepared at T_{dep} = 989 K at several measurement temperatures. Solid lines represent curve fittings from the equivalent R–CPE–C parallel circuit. Arrows indicate the peak positions of the imaginary electric modulus as a function of frequency.

$$\omega_{peak} = \frac{1}{RC} \tag{4}$$

The slightly lower peak frequency of Z'' than that of M'' has often been observed in actual materials. The R–CPE–C model fitted the frequency dependence and peak shifts of Z'' and M'' (solid lines in Fig. 5).

Adequacy of the R-CPE-C model will be discussed in comparison with other possible models. Fig. 6 shows the calculated impedance responses for five equivalent circuit models listed in Table 1, namely RC, RC + RC, R-CPE, C-CPE and R-CPE-C. The open symbols correspond to the experimental data for the (0 2 0)-oriented $BaTi_2O_5$ film prepared at T_{dep} = 989 K and measured at 905 K. The single RC parallel circuit (RC) model gives a Debye-type response in the Z^* and M^* complex plane

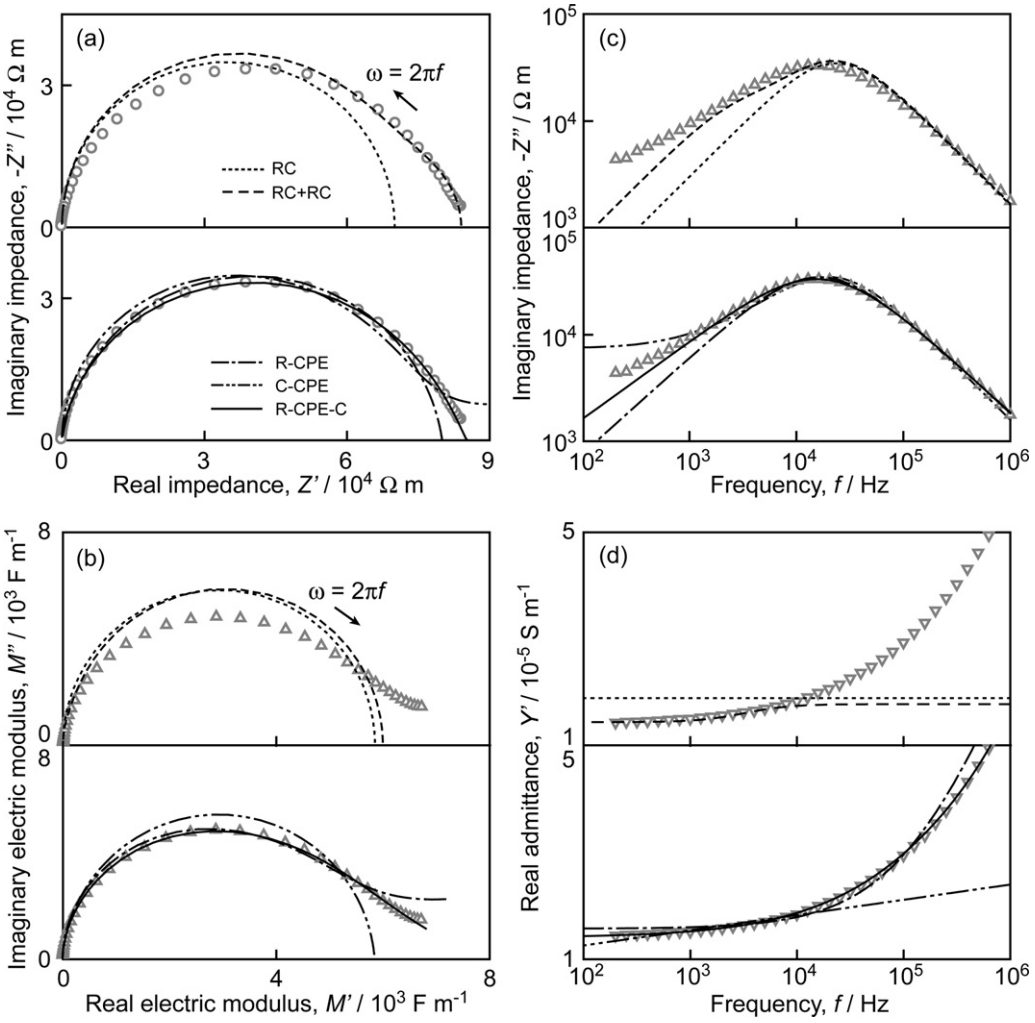

Fig. 6. Impedance (a) and electric modulus (b) complex plane plots and imaginary impedance (c) and real admittance (d) spectroscopic plots for the (0 2 0)-oriented $BaTi_2O_5$ film prepared at T_{dep} = 989 K measured at 905 K (open symbols). Calculated curves represent the equivalent electrical circuit models of single RC (dotted lines), RC + RC (dashed lines), R–CPE (chain lines), C–CPE (two-dot chain lines) and R–CPE–C (solid lines).

Table 1
Equivalent circuit models and parameters used for the calculations.

Model	Circuit	R/Ω m	C/F m^{-1}	Q/S s^n	n
RC	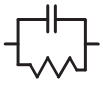	70,000	1.0×10^{-10}	–	–
RC + RC	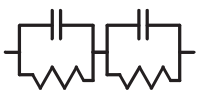	70,000	1.0×10^{-10}	–	–
		14,000	4.0×10^{-9}		
R–CPE		80,000	–	3.5×10^{-10}	0.91
C–CPE		–	1.0×10^{-10}	8.0×10^{-6}	0.05
R–CPE–C		85,000	7.5×10^{-11}	3.0×10^{-9}	0.66

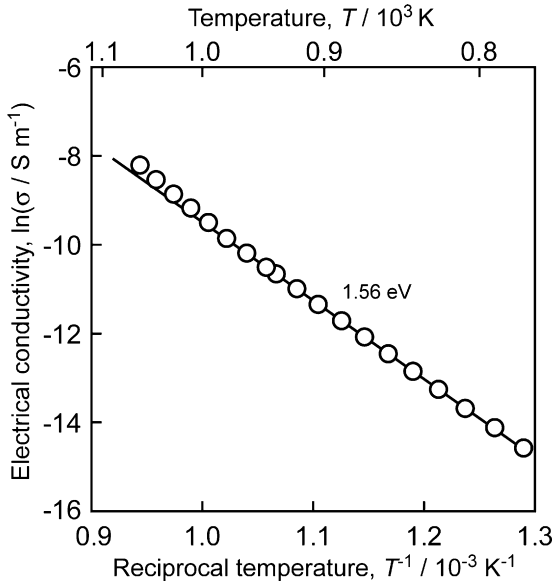

Fig. 7. Temperature dependence of the electrical conductivity of the (0 2 0)-oriented $BaTi_2O_5$ film prepared at T_{dep} = 989 K.

plots (dotted lines in Fig. 6(a) and (b), respectively). The RC model also shows a single Debye peak in the plot of Z'' against frequency (dotted line in Fig. 6(c)) and a flat Y' response independent of frequency (dotted lines in Fig. 6(d)). The serial RC parallel circuit (RC + RC) model may illustrate a distorted semicircular shape in the Z^* plane plot, in which two semicircular components might have been combined into one distorted semicircle assuming a series combination of bulk and grain boundary contributions. The RC + RC model fits the data better than the single RC model by adding another semicircular component in the Z^* response in the low frequency range (dashed lines in Fig. 6(a) and (c)). However, the RC + RC model cannot explain the depressed semicircular shape in the M^* complex plane plot as well as RC model (dashed line in Fig. 6(b)). Especially, two RC components resulted in two plateaus in Y' spectroscopic plot (dashed line in Fig. 6(d)).

The non-Debye-type CPE has often been introduced to reproduce the experimental results. We calculated results for two models with the CPE in parallel combination with either C (C-CPE) or R (R-CPE) (two-dot chain lines and chain lines in Fig. 6, respectively). The parameters used for the calculation are listed in Table 1. Despite the good fittings for Z^* complex plane plots, the C–CPE and R–CPE models still showed Debye-like behavior on the M^* complex plane and the Z'' and Y' spectroscopic plots (Fig. 6(b)–(d)). Here, we assume the Z'', M'', and Y^* responses for the R–CPE–C model as obtained in the following Eqs. (5)–(7)[15]:

$$Z''_{\text{R–CPE–C}} = \frac{B\omega^n + \omega C}{(1/R + A\omega^n)^2 + (B\omega^n + \omega C)^2}, \quad (5)$$

$$M''_{\text{R–CPE–C}} = \frac{C_0}{C}\frac{\omega C(1/R + A\omega^n)}{(1/R + A\omega^n)^2 + (B\omega^n + \omega C)^2}, \quad (6)$$

$$Y^*_{\text{R–CPE–C}} = 1/R + jC\omega + A\omega^n + jB\omega^n, \quad (7)$$

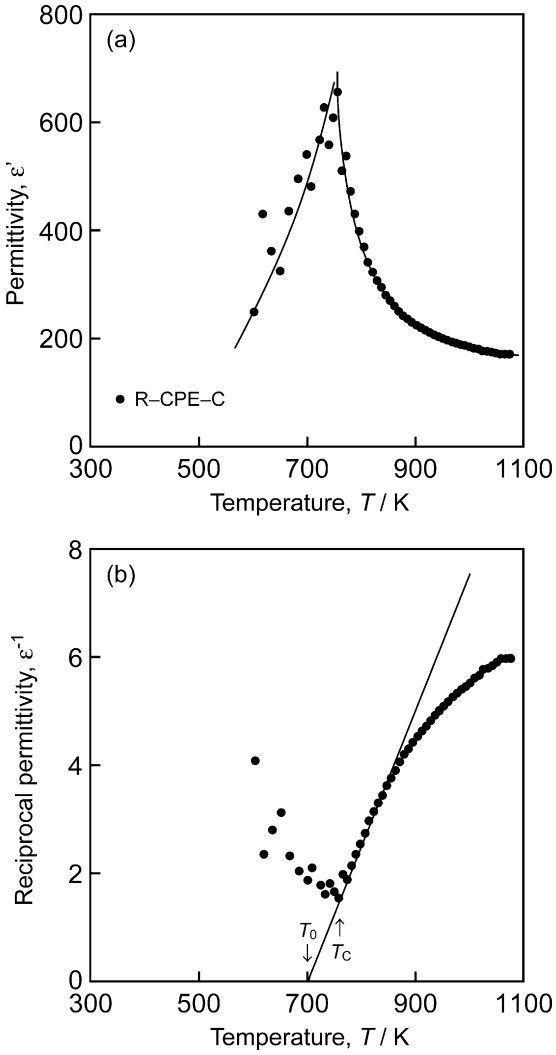

Fig. 8. Temperature dependence of ε' for the (0 2 0)-oriented $BaTi_2O_5$ film prepared at T_{dep} = 989 K that determined from the R–CPE–C equivalent circuit parameters (a), temperature dependence of the reciprocal permittivity (b). T_0 and T_C refer to the Curie–Weiss and Curie temperatures, respectively.

where A and B are the arbitrary constants corresponding to the real and imaginary parts of the CPE, respectively. In the R–CPE model listed in Table 1, by substituting $C = 0$ and $n = 0.91$ in Eq. (5), Z'' frequency dependence mostly reduces to the simple RC model. In the C–CPE model, by substituting $R = \infty$ and $n = 0.05$ in Eqs. (6) and (7), M'' frequency dependence mostly reduces to the simple RC model and the Y' response follows a power law as a function of frequency. As a result, the C–CPE and R–CPE models still showed Debye-like behavior against frequency and cannot reproduce the experimental results totally.

The R–CPE–C parallel circuit model, which had an intermediate n value of 0.66, reproduced the experimental results well (solid lines in Fig. 6). The chi-squared goodness of fit was significantly small ranging from 10^{-4} to 10^{-5} above 734 K. The R–CPE–C parallel circuit model also reproduced the frequency dependence of the interrelated behaviors of Z^*, M^*, and Y^* on the complex plane and the spectroscopic plots. Therefore, this model is adequate to represent the dielectric response of the present $BaTi_2O_5$ film as well as the $BaTi_2O_5$ single crystal.[15]

Table 2
Permittivity (ε'), Curie temperature (T_C), Curie–Weiss temperature (T_0), and activation energy (E_a) for $BaTi_2O_5$ in single-crystal, polycrystalline body and film forms.

	ε'	T_C (K)	T_0 (K)	E_a (eV)	Ref
Single crystal					
Floating zone	20500	748	747	1.50	1
Solution growth	30000	703	692		24
Floating zone	20000	748	724–735	1.13	14
Polycrystalline body					
Pressureless	130	748	–	1.58	30
SPS	580	703	–	–	31
Hot press	300	723	574	1.57	2
Arc melting	1800	750	700	1.37	2
Film					
Laser ablation	2000	750	–	–	10
Laser CVD	653	759	701	1.56	

Figs. 7 and 8 depict the temperature dependence of electrical conductivity and relative permittivity (ε') of the (0 2 0)-oriented $BaTi_2O_5$ film prepared at T_{dep} = 989 K. The activation energy (E_a) at temperatures between 775 and 1000 K was 1.56 eV. The (0 2 0)-oriented $BaTi_2O_5$ film had ε' = 98–113 at room temperature. With increasing temperature, ε' increased and showed maxima around 760 K. The ε' calculated from the R–CPE–C model had a maximum value of ε' = 653 at 759 K. Its reciprocal (ε'^{-1}) plot obeyed the Curie–Weiss law at temperatures above 750 K (Fig. 8(b)), and T_C and Curie–Weiss temperature (T_0) were 759 and 701 K, respectively. Dielectric loss ($\tan\delta$) ranged between 0.02 and 0.05 below 600 K and increased with increasing temperature above 600 K. The ferroelectric phase transition of $BaTi_2O_5$ is still controversial. According to the crystal structure refinement of $BaTi_2O_5$[25], the displacement of Ti atoms in the Ti1 sites is mainly responsible for the ferroelectricity. Hushur et al. suggested an order-disorder phase transition around T_C by using Raman and Brillouin scattaering spectra.[32] Yashima et al. refined the high-temperature $BaTi_2O_5$ phase by high-temperature neutron diffraction and reported that the displacement of constituent atoms along the *b*-axis resulted in the phase transition from low-temperature ferroelectric *C*2 to high-temperature paraelectric *C*2/*m* phase.[33]

Table 2 summarizes the dielectric properties (ε', T_C, T_0, and E_a) of $BaTi_2O_5$ in its single-crystal, polycrystalline body and film forms. ε' of the $BaTi_2O_5$ single crystal along the *b*-axis was more than 20,000 and its T_C was 703–748 K.[1,14,24] $BaTi_2O_5$ sintered bodies had a relatively low ε' of 130–580.[2,30,31] The $BaTi_2O_5$ body prepared by arc melting showed *b*-axis orientation, and thus it had a high ε' among polycrystalline bodies.[2] E_a was almost agreed with that of the present study.

4. Conclusions

Single-phase $BaTi_2O_5$ thick films were prepared on Pt-coated Si substrates by laser CVD. (0 2 0)-oriented $BaTi_2O_5$ films were obtained at $m_{Ti/Ba}$ = 1.72–1.74 and T_{dep} = 989–1051 K. A rhombic terrace formed on the surface of (0 2 0)-oriented $BaTi_2O_5$ films, and the inner angle of the terrace corresponded to the crystal structure of monoclinic $BaTi_2O_5$. The deposition rate of $BaTi_2O_5$ films was approximately 90 $\mu m\,h^{-1}$. The ac impedance response of (0 2 0)-oriented $BaTi_2O_5$ films was interpreted using equivalent circuits composed of parallel elements of R, C and the CPE.

Acknowledgments

This work was supported in part by the Global COE Program of Materials Integration, Tohoku University, the ICC-IMR Program at Tohoku University, the International Science and Technology Cooperation Program of China (No. 2009DFB50470), JSPS Grant-in-Aid for Young Scientists (B) (No. 22760550), and MEXT Grant-in-Aid for Scientific Research (A) (No. 22246082).

References

1. Akashi T, Iwata H, Goto T. *Mater Trans* 2003;**44**:802–4.
2. Tu R, Goto T. *Mater Trans* 2006;**47**:2898–903.
3. Waghmare U, Sluiter MHF, Kimura T, Goto T, Kawazoe Y. *Appl Phys Lett* 2004;**84**:4917–9.
4. Scott JF, Paz de Araujo CA. *Science* 1989;**246**:1400–5.
5. Ngo E, Joshi PC, Cole MW, Hubbard CW. *Appl Phys Lett* 2001;**79**:248–50.
6. Wang Z, Miao J, Zhu W. *J Eur Ceram Soc* 2007;**27**:3759–64.
7. Liao M, Imura M, Fang X, Nakajima K, Chen G, Koide Y. *Appl Phys Lett* 2009;**94**:242901.
8. Krieger JH. *J Appl Phys* 2009;**105**:061629.
9. Yu O, Andrey G, Kaul R, Wahl G. *Chem Vapor Depos* 2004;**3**:193–6.
10. Wang CB, Tu R, Goto T. *J Vac Sci Technol* 2007;**25**:304–7.
11. Banal R, Kimura T, Goto T. *Mater Trans* 2005;**46**:2114–6.
12. Ito A, Kadokura H, Kimura T, Goto T. *J Alloy Compd* 2010;**489**:469–74.
13. Ito A, Endo J, Kimura T, Goto T. *Surf Coat Technol* 2010;**204**:3846–50.
14. Jonscher AK. *J Mater Sci* 1978;**13**:553–62.
15. Masó N, Yue XY, Goto T, West AR. *J Appl Phys* 2011;**109**:024107.
16. Statton WO. *J Chem Phys* 1951;**19**:33–40.
17. Rase DE, Roy R. *J Am Ceram Soc* 1955;**38**:102–13.
18. Negas T, Roth RS, Parker HS, Minor D. *J Solid State Chem* 1974;**9**:297–307.
19. O'Bryan HM, Thomson J. *J Am Ceram Soc* 1974;**57**:522–6.
20. Jonker GH, Kwestroo W. *J Am Ceram Soc* 1958;**41**:390–4.
21. Guha JP. *J Am Ceram Soc* 1977;**60**:246–9.
22. Ritter JJ, Roth RS, Blendell JE. *J Am Ceram Soc* 1986;**69**:155–62.
23. Kirby KW, Wechsler A. *J Am Ceram Soc* 1991;**74**:1841–7.
24. Akishige Y. *Jpn J Appl Phys* 2005;**44**:7144–7.
25. Kimura T, Goto T, Yamane H, Iwata H, Kajiwara T, Akashi T. *Acta Crystallogr C* 2003;**59**:128–30.
26. Zhu N, West AR. *J Am Ceram Soc* 2009;**93**:295–300.
27. Javadpour J, Eror NG. *J Am Ceram Soc* 1988;**71**:206–13.

28. Tohma T, Masumoto H, Goto T. *Mater Trans* 2002;**43**:2880–4.
29. Kwak BS, Zhang K, Boyd EP, Erbil A, Wilkens BJ. *J Appl Phys* 1991;**69**:767–72.
30. Beltrán H, Gómez B, Masó N, Cordoncillo E, Escribano P, West AR. *J Appl Phys* 2005;**97**:084104.
31. Akishige Y, Xu J, Shigematsu H, Morito S, Ohba T. *Jpn J Appl Phys* 2009;**48**:051402.
32. Hushur A, Shigematsu H, Akishige Y, Kojima S. *Appl Phys Lett* 2005;**86**:112903.
33. Yashima M, Tu R, Goto T, Yamane H. *Appl Phys Lett* 2005;**87**:101909.